AGU PUBLICATIONS

JGR

Journal of Geophysical Research: Space Physics

RESEARCH ARTICLE
10.1002/2016JA023281

Key Points:
- The rotational modulations of Saturn radio emissions are different in each hemisphere and vary over a Saturn year
- The rotation rate of northern SKR became slower than that of southern SKR in 2015
- The phase difference between SKR and auroral hiss and the intensity of auroral hiss are local time dependent

Correspondence to:
S.-Y. Ye,
shengyi-ye@uiowa.edu

Citation:
Ye, S.-Y., G. Fischer, W. S. Kurth, J. D. Menietti, and D. A. Gurnett (2016), Rotational modulation of Saturn's radio emissions after equinox, *J. Geophys. Res. Space Physics*, *121*, 11,714–11,728, doi:10.1002/2016JA023281.

Received 3 AUG 2016
Accepted 5 NOV 2016
Accepted article online 11 NOV 2016
Published online 3 DEC 2016

Rotational modulation of Saturn's radio emissions after equinox

S.-Y. Ye[1], G. Fischer[2], W. S. Kurth[1], J. D. Menietti[1], and D. A. Gurnett[1]

[1]Department of Physics and Astronomy, University of Iowa, Iowa City, Iowa, USA, [2]Space Research Institute, Austrian Academy of Sciences, Graz, Austria

Abstract Saturn kilometric radiation (SKR), narrowband emission, and auroral hiss are periodically modulated due to Saturn's rotation, and the periods were found to vary with time. We analyze Cassini observations of Saturn's radio emissions with the main focus on the four years 2012–2015. It is shown that the rotation rates of SKR north and south were different since mid-2012 with SKR north being faster until autumn 2013, followed by a 1 year interval of similar north and south rotation rates and phases, before the northern SKR component finally became slower than the southern SKR in late 2014. The dual rotation rates of 5 kHz narrowband emissions reappeared for slightly longer than 1 year after a long break since equinox. Auroral hiss provides an unambiguous way of tracking the rotation signals from each hemisphere because the whistler mode waves cannot cross the equator. Rotation rates of auroral hiss and narrowband emissions are consistent with each other and those of SKR when they are observed at high latitudes in early 2013. The phase difference between SKR and auroral hiss and the intensity of auroral hiss are local time dependent.

1. Introduction

Due to the lack of trackable surface features, the rotation rates of gas giant planets have been determined based on the modulation of auroral radio emissions, which are emitted on auroral field lines by an electron population unstable to the cyclotron maser instability [*Wu and Lee*, 1979]. The International Astronomical Union longitude system adopted for Saturn was based on the period of Saturn kilometric radiation (SKR) measured by Voyager [*Desch and Kaiser*, 1981]. Later observations by Ulysses and Cassini spacecraft revealed substantial variations of the SKR period [*Lecacheux et al*., 1997; *Galopeau and Lecacheux*, 2000; *Gurnett et al*., 2005]. *Kurth et al*. [2007, 2008] developed a longitude system for Saturn based on the Cassini Radio and Plasma Wave Science (RPWS) measurement of the variable SKR period. The radio rotation rate of Saturn has also been found to consist of two components [*Kurth et al*., 2008], one associated with each hemisphere [*Gurnett et al*., 2009a]. The dual rotation rates are also observed in Saturn narrowband emission and auroral hiss, which are modulated at the planetary rotation periods [*Gurnett et al*., 2009b; *Ye et al*., 2010a].

Many of the periodic variations observed in Saturn's magnetosphere can be associated with the field-aligned currents that couple the polar ionosphere to the magnetosphere [*Southwood and Cowley*, 2014; *Kivelson and Jia*, 2014]. The variable SKR periods [*Galopeau and Lecacheux*, 2000; *Gurnett et al*., 2005] and the time variability in the magnetic field oscillations [*Andrews et al*., 2008, 2011, 2012] indicate that the magnetic field and field-aligned currents are slipping over the neutral atmosphere in the polar region. This is because the variation of 1% in the rotation period over a few decades is too large to arise from the deep interior due to the massive moment of inertia of Saturn [*Gurnett et al*., 2007]. *Smith* [2006] suggested that the changing neutral wind in the auroral zone should have an influence on the slippage of the magnetosphere. The seasonal changes in wind speeds and Pedersen conductivities in the auroral ionosphere could influence the ionosphere-magnetosphere coupling currents, which lead to time variability and hemispheric asymmetry in the SKR periods [*Gurnett et al*., 2009a].

Based on RPWS observations of SKR before equinox (2004–2010), *Kimura et al*. [2013] showed that SKR intensity is correlated with both solar EUV flux and solar wind dynamic pressure. This confirms the long-term control of SKR by the seasonal solar EUV flux and solar wind pressure, which varies within a solar cycle. Recently, *Provan et al*. [2015] showed that the abrupt changes in the planetary period oscillations might be related to the contraction and expansion of Saturn's magnetosphere in response to the changes in the upstream solar wind conditions. Previously, *Zarka et al*. [2007] also observed a correlation between the short-term variation of SKR periods and the solar wind speed.

The variable rotation rate of Saturn's magnetosphere was also revealed by observations of magnetic fields and charged particles [*Andrews et al*., 2010a, 2010b, 2012; *Provan et al*., 2011, 2012, 2013; *Carbary et al*., 2009, 2011]. The oscillation of the locations of the UV aurora, magnetopause, and bow shock was also found to be related to the modulation of the magnetic field and plasma inside the magnetosphere of Saturn [*Nichols et al*., 2008, 2010a, 2010b; *Clarke et al*., 2006, 2010a, 2010b]. *Rymer et al*. [2013] suggested that the variable mass loading from the moon Enceladus could affect the rotation rate of Saturn's magnetosphere. One of the advantages of using radio emissions to track the rotational rates of the planets is that these free space-propagating waves can be observed from far away and therefore the observation is nearly continuous. In contrast, the modulation of magnetic field components can only be observed during each periapsis pass.

In this paper, we will extend the periodicity analysis of the Saturn radio emissions and plasma waves beyond Saturn's equinox in 2009 to late 2015. In the following sections, we will analyze the rotational modulation of SKR, narrowband emissions, and auroral hiss respectively using the Lomb-Scargle period analysis [*Lomb*, 1976; *Scargle*, 1982] (also known as least squares spectral analysis, similar to the tracking filter analysis method described by *Gurnett et al*. [2011a]) and a phase tracing method [*Kurth et al*., 2007, 2008].

2. Saturn Kilometric Radiation

SKR is emitted by unstable populations of electrons on auroral field lines via the cyclotron maser instability [*Wu and Lee*, 1979]. The SKR intensifies periodically when the rotating asymmetrical ring current of Saturn passes through the early morning LT sector [*Mitchell et al*., 2009], causing enhancement of field-aligned currents that drive the auroral process [*Lamy et al*., 2010; *Kurth et al*., 2011; *Menietti et al*., 2011]. In the classical picture SKR is mainly modulated like a clock, which means that the timing of the intensification of SKR is not affected by the observer's local time [*Warwick et al*., 1981]. Recent studies [*Lamy*, 2011; *Andrews et al*., 2011; *Lamy et al*., 2013; *Cowley and Provan*, 2016] suggest that the SKR modulation is fundamentally a rotating system in phase with the upward going field-aligned current of the rotating current system. However, over large regions of the observer's local time (03–12 LT) SKR still appears clocklike [*Andrews et al*., 2011], and the appearance is also clock like with Cassini on the afternoon side as long as the spacecraft apoapsis, during which most of the SKR is recorded, is not changing much [*Fischer et al*., 2015]. The latter is due to the beaming of SKR whose source local time stays the same over several Saturn rotations (thereby mimicking a clock-like source) when the observer's position is relatively constant during apoapsis. The SKR observed from the afternoon side should experience a phase shift with respect to the morning side SKR, which is described by the model of *Andrews et al*. [2011] or *Cowley and Provan* [2016]. Cassini apoapsis was on the afternoon side in 2012 until mid-2013 varying only in the range of 14–18 LT, but it experienced a shift over midnight to the morning side during the second half of 2013. From early 2014 to the end of 2015 the location of the spacecraft was on the morning side (03–08 LT) in the SKR clocklike region. Thus, similar to previous studies, no correction for the observer's local time is employed here. The modulation rate (ω) of SKR can be obtained by maximizing the peak-to-peak power when we fit the SKR power to a sine function of the longitude of the Sun (ωt). A detailed description of this tracking filter analysis method can be found in *Gurnett et al*. [2011a].

Gurnett et al. [2009a] applied the tracking filter analysis to the SKR signals observed in the northern and southern hemispheres by separating the observations by latitude and showed a clear asymmetry in the rotational modulation period of SKR between hemispheres. It was found that the southern SKR had a period of ~10.8 h (rotation rate of 800°/d) from 2004 to 2009, whereas the northern SKR had a period of ~10.6 h (rotation rate of 815°/d) from 2006 to 2009. These two periods started to converge in 2009 and by 2010, several months after equinox, seemed to have merged [*Gurnett et al*., 2010a].

The modulation rates of SKR after equinox have since been studied by *Fischer et al*. [2015], who used a phase tracing method [*Kurth et al*., 2007, 2008] to reveal the short-term variation of SKR periodicities. They showed that the north and south SKR periods crossed each other briefly after equinox and remained phase locked (same period) from spring 2010 up to mid-2012, except for the first few months of 2011. The brief phase separation between the northern and southern SKR in 2011 might have been caused by the Great White Spot (GWS). This super lightning storm of Saturn could have perturbed the polar ionosphere of the planet, disrupting the phase lock between hemispheres [*Fischer et al*., 2014].

Figure 1 shows the rotational modulation spectrograms of SKR, where the modulation power of SKR is plotted as a function of rotation rate and time. The intensities of SKR, integrated between 80 and 500 kHz,

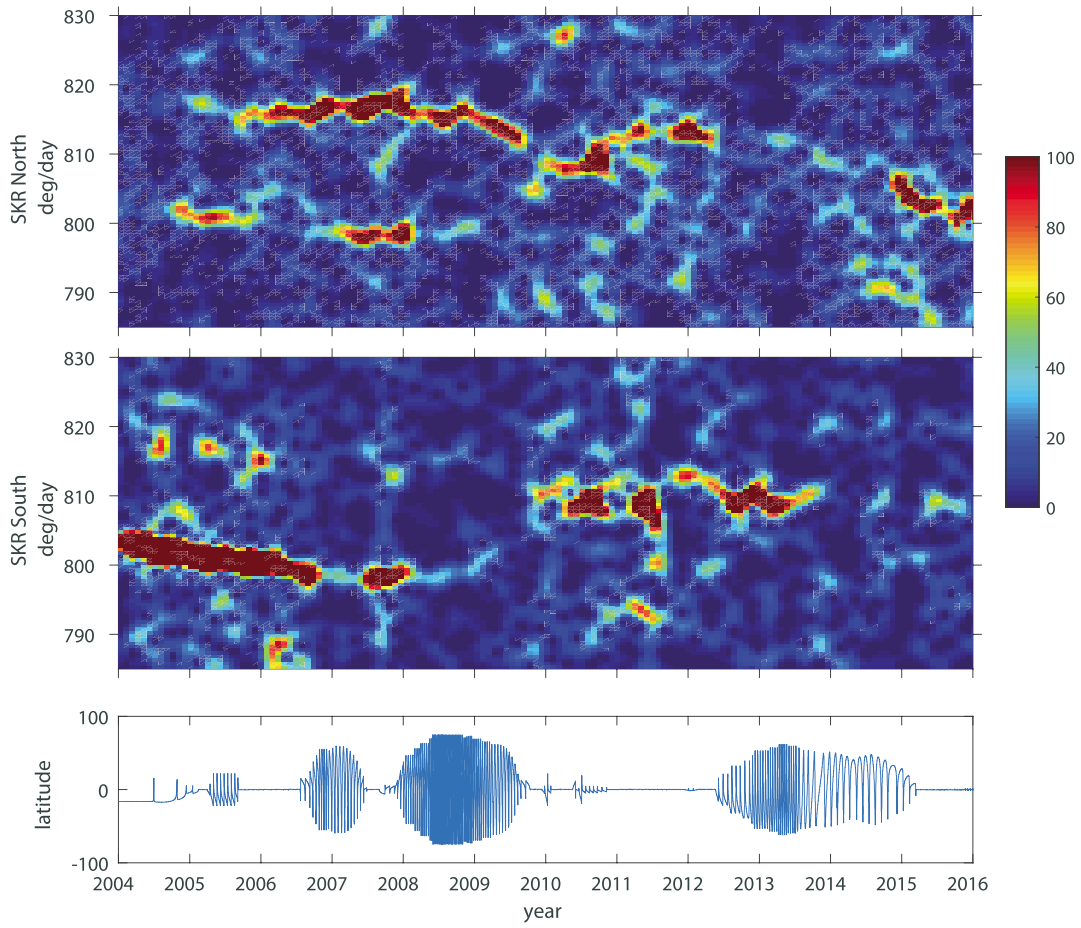

Figure 1. Lomb-Scargle modulation spectrograms of the (top) north and (middle) south SKR power (separated by polarization), observed from year 2004 to 2016. The color indicates the Lomb normalized modulation power with red (100) indicating strong modulation and blue (0) indicating no modulation. (bottom) The latitude of Cassini is also shown.

are separated by their hemispherical origin according to the sense of circular polarization. The integrated power values are then averaged within 10 min windows and divided by the running average (65 samples, about one rotation of Saturn) to remove the orbital distance effect on the power level. The modulation spectral powers shown in Figure 1 are calculated by a fast Lomb algorithm [*Press*, 2007] from these relative intensities. Figure 1 shows the Lomb normalized modulation of north (top) and south (middle) SKR power. The color bar is such that red (100) indicates strong modulation and blue (0) indicates no modulation. These numbers can be converted to statistical significance levels of the modulation signals. The north SKR modulation signals are largely absent from mid-2012 to late 2014. There are only three weak signals at ~812°/d (spring 2013), at ~809 to 808°/d (late 2013/early 2014), and at ~809°/d (autumn 2014). The south SKR modulation signals are absent after late 2013 before they reappear in mid-2015. One of the main reasons for this behavior is the Cassini high-latitude trajectory from mid-2012 to early 2015. Until late 2013 Cassini spent most of its time at high southern latitudes where south SKR is visible. This gradually changed to more time spent at northern midlatitudes, from where north SKR is visible. The latest data, from the end of 2014 to the end of 2015, show that the north SKR rotation rate has decreased to ~802°/d, whereas the south SKR rotation rate remained at ~808°/d, although its rotation signal is relatively weak. In 2015, Cassini was mostly in the equatorial plane of Saturn.

From the phase plots of SKR power separated by hemisphere, we can determine that the north and south SKR rotation rates and phases come close to each other in late 2013. In the phase plots (Figure 2), the integrated wave powers have been normalized by the average value of each planetary rotation. The color code is such that white means wave power much more intense than the average and black means much weaker than

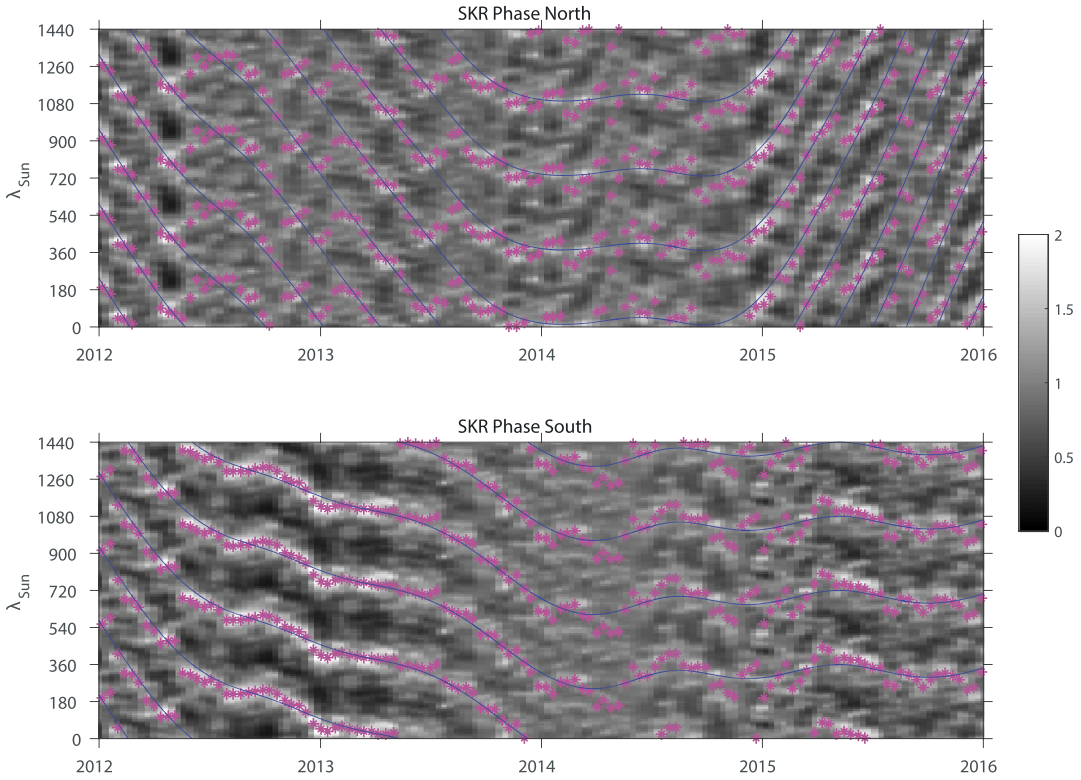

Figure 2. Phase diagrams for the (top) north and (bottom) south SKR, separated by polarization, observed from year 2012 to 2016. The intensities are normalized by the averaged intensity over one rotation (360°), and this ratio is displayed in gray scales according to the bar on the right side. White indicates wave power much more intense than the average and black indicates wave power much weaker than the average. Blue lines show the ways the computer traced the intensity maxima of the north and south SKR. The longitude of the Sun (λ_{Sun}) is calculated based on a fixed guiding rate of 808°/d. The magenta star symbols are calculated by directional statistics, and they are basically periodic averages of SKR phases weighted by SKR intensity.

the average. The slope of the drifting SKR phase, determined by connecting the high SKR intensities in the phase-time plot, reveals the SKR modulation rates relative to the guide rate (arbitrarily chosen as 808°/d). The rotation rate is simply the slope of the drifting SKR phase (in °/d) subtracted from the guide rate, and corresponding mathematical equations can be found in Appendix C of *Fischer et al.* [2015]. A positive slope means that the SKR rate is slower than the guide rate, and a negative slope means that the SKR rate is faster than the guide rate. For the north SKR, it is difficult to trace its phase in Figure 2 from mid-2012 to late 2014 because the wave power seems to be modulated at two different rotation rates, whereas for the south SKR it is easy to follow the phase until late 2013. Note that there might be slightly different ways how one can interpret the phase drift of SKR. The rotation rates inferred from the phase drift interpretation will vary accordingly. Our SKR phase tracing was guided by directional statistics (magenta star symbols in Figure 2). The directional statistics are basically periodic averages of SKR phases weighted by SKR intensity. *Fischer et al.* [2015] have shown that the SKR rotation rates determined this way agree with the modulation signals in the SKR modulation spectrogram calculated using tracking filter method up till the end of 2012. For 2015 we have a clear indication for two SKR periods also in the tracking filter analysis of Figure 1 with the south SKR rate being faster than the northern one. It is actually not the first time after Saturn equinox that the south SKR is faster. A careful inspection of Figure 1 shows that this was already the case for a few months in 2009, confirming the finding of *Fischer et al.* [2015] that the periods crossed for a few months after equinox. For late 2009, Figure 1 shows a north SKR modulation signal at ~804°/d, whereas the south SKR has a signal at ~811°/d, and both signals merge in spring 2010. Two SKR rotation rates are also present for a few months in spring/summer 2011 (followed by merging of periods in September 2011), but in that time interval the rate in the north is faster than the south.

Until late 2013 the slope of SKR north looks steeper (more negative) than for SKR south indicating a faster SKR north rate. The slope of SKR north is negative (consistent with 812°/d) in spring 2013 and turns horizontal in

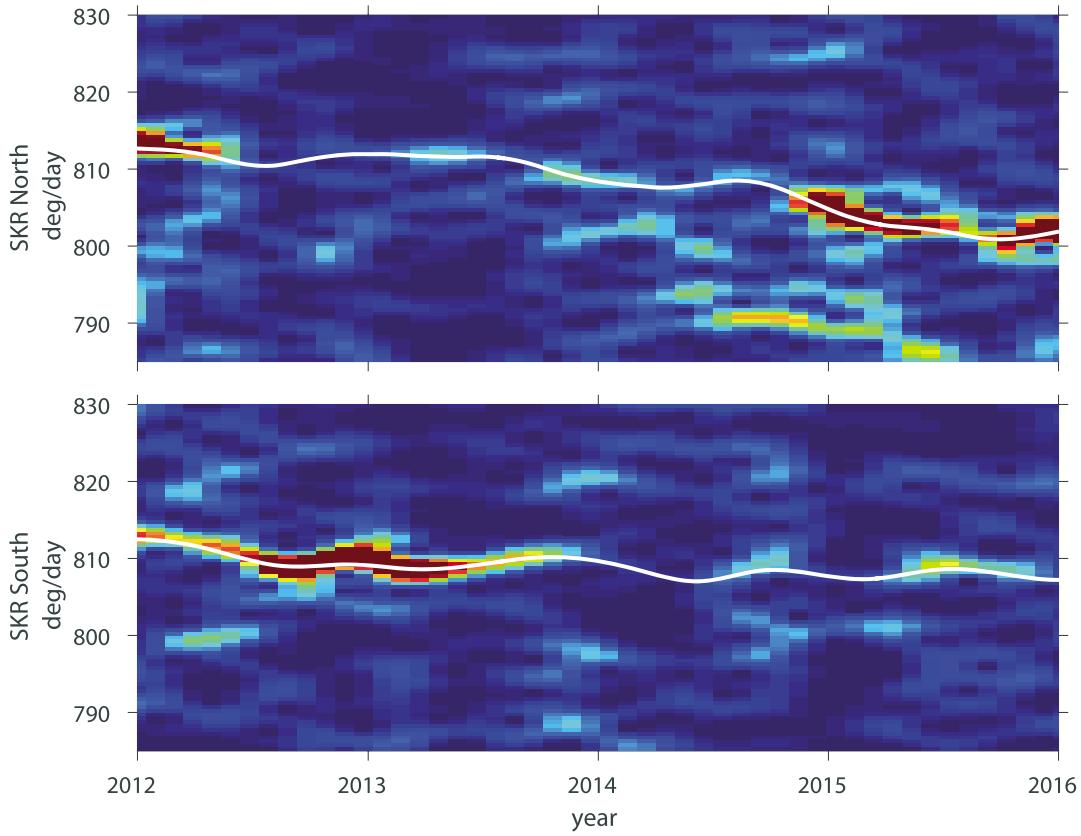

Figure 3. Comparison of rotation rates of north and south SKR derived from semiautomatic phase tracing (white lines) with the rotational modulation spectrograms (derived from Lomb-Scargle analysis). The color scale of the spectrograms is the same as that of Figure 1.

late 2013 (808°/d) and clearly positive in late 2014. The phase slope of SKR south is similar to that of SKR north until mid-2012, indicating similar modulation periods. From mid-2012 to late 2013, the SKR south phase slope is less negative than that of SKR north, which means that the rotation rate SKR north is higher than the south. After late 2013, both SKR north and south phases turn flat, which means similar rotation rates for the north and south around 808°/d. The divergence of the SKR periods took place in late 2014 with the SKR north phase slope turning positive while the SKR south phase stayed approximately flat, which indicates a slower SKR north rotation rate afterward. Except for a brief crossing of SKR periods right after equinox [*Fischer et al*., 2015], this is the first instance of a slower northern SKR rotation throughout the Cassini mission, during which the south SKR rotation was mostly slower. One might suggest a different path how the SKR phases are evolving and derive the corresponding rotation rates from the slopes, but the current phase tracing was done with the guidance of the directional statistics and the resulting rotation rates are consistent with the tracking filter analysis result, as shown in Figure 3.

We used a semiautomatic procedure for tracing the SKR phases. The calculation of directional statistics was done as described in Appendix C of *Fischer et al*. [2015], but with time steps of 12 days (between the magenta points in Figure 2). To get the blue line in Figure 2, we performed a running average over nine directional statistic phase data points three times to smooth out the kinks and wiggles. (Some data points needed a phase correction by adding or subtracting 360° before the running average to follow the general trend of the SKR maximum phases. This avoids kinks and deviations from the rotation rates of the Lomb-Scargle method, and this is the only nonautomated part of the whole procedure.) To eliminate the edge effect in the running average, we included data 90 days before day of year (DOY) 001, 2012, and 90 days after DOY 001, 2016. We also tried different time steps for the directional statistics varying from 4 to 18 days. Small time steps led to many wiggles in the curves, whereas large time steps led to smooth curves sometimes quite far away from the SKR maximum. Figure 3 shows that 12 days is a good choice

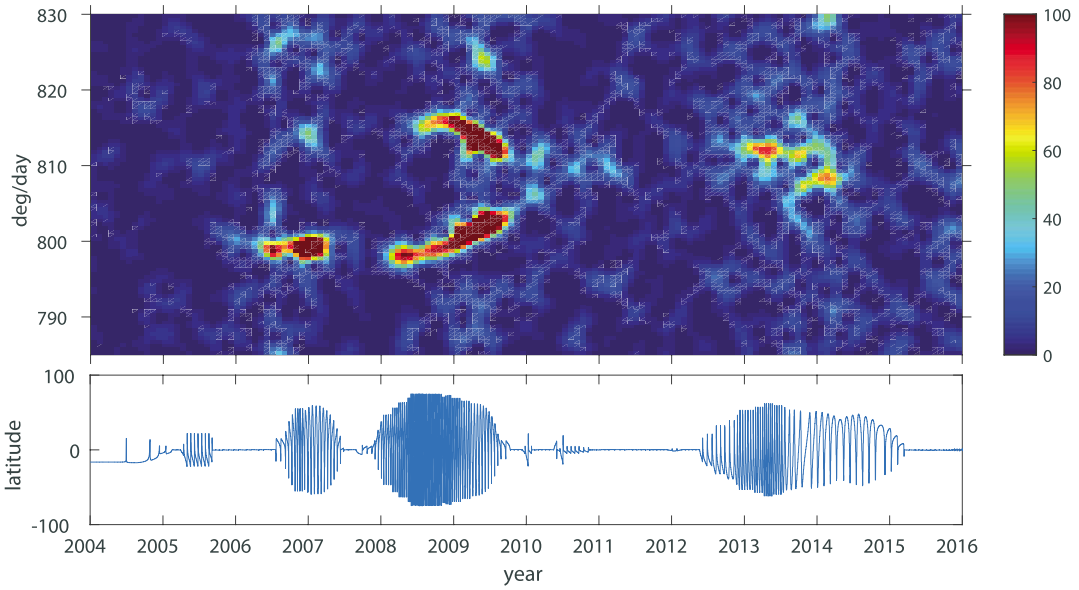

Figure 4. Lomb-Scargle modulation spectrogram of the 5 kHz narrowband emission observed from year 2004 to 2016. The color shows the Lomb normalized modulation power, same as Figure 1. The latitude plot of Cassini shows that the modulation signal is preferably observed during high inclination orbits.

and that the temporal derivative of our SKR phase tracing results in rotation rates consistent with the Lomb-Scargle method.

3. Narrowband Emission

Saturn narrowband emissions are mode converted *L-O*-mode emissions most prominently observed around 5 kHz [*Wang et al.*, 2010]. Less intense narrowband emissions are observed at higher frequencies (~10–70 kHz) and are found to originate from upper hybrid resonance emissions on the boundary of the plasma torus [*Ye et al.*, 2009; *Menietti et al.*, 2009]. During the perikrones of Cassini's high inclination orbits in 2008, where the local plasma frequency is lower than the local electron cyclotron frequency, RPWS observations showed that the narrowband emissions are first generated as *Z*-mode emissions before mode conversion to *L-O* mode [*Ye et al.*, 2010b]. This is supported by the wave growth calculation of *Z*-mode narrowband emissions (~20 kHz) based on the electron phase space distribution measured in the source region [*Menietti et al.*, 2010].

Wang et al. [2010] showed that 5 kHz narrowband emissions are modulated like a clock. *Ye et al.* [2010a] studied the rotational modulation of the Saturn narrowband emission for the period between Saturn orbit insertion and equinox and revealed the dual periodicity of 5 kHz narrowband emissions, which are identical to the northern and southern SKR periods. In contrast to SKR, both modulation periods of narrowband emissions are observable in each hemisphere. If we restrict the narrowband emission data set to one hemisphere by limiting the latitude of observation, both north and south rotation signals still exist no matter which hemisphere we look at. This is due to the fact that narrowband emissions are originally generated as *Z*-mode emission, which is trapped in a region close to Saturn bounded by the upper hybrid frequency and the *Z*-mode cutoff frequency contour. Therefore, these *Z*-mode emissions can cross the equator before they convert to *L-O* mode and escape.

Figure 4 shows the Lomb-Scargle modulation spectrogram of the 5 kHz narrowband emission from 2004 to the end of 2015. Notice that the modulation signals are most intense during the high inclination orbits of Cassini (2006–2007, 2008, 2009, and 2013; see Cassini latitude plot in Figure 1). The dual periods of narrowband emissions converged before the equinox and seemed to merge into one period after, although the rotational modulation signals after equinox are relatively weak. This convergence of dual periods into one is consistent with the SKR periodicities analyzed by *Fischer et al.* [2015]. The slowing down of the narrowband

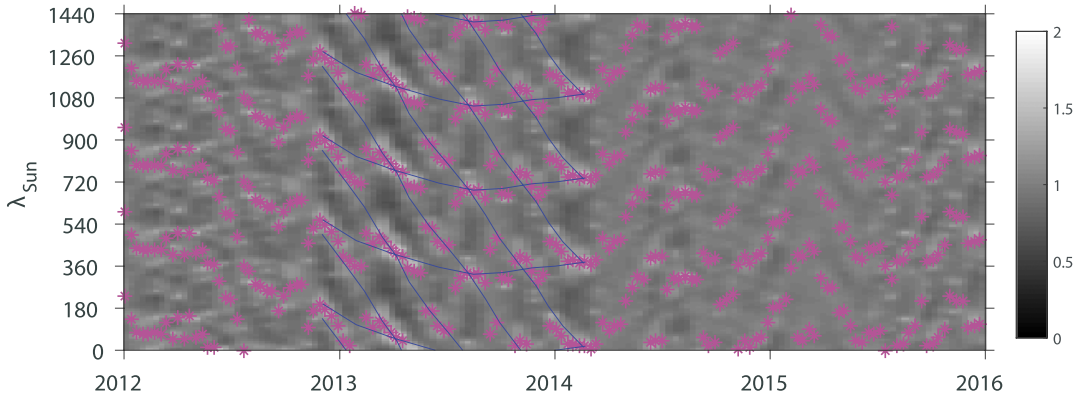

Figure 5. Phase plot of 5 kHz narrowband emissions (guiding rate 808°/d) between year 2012 and 2016. Blue lines indicate two possible ways of tracing the intensity maxima of the narrowband emission. The longitude of the Sun is calculated based on a fixed guiding rate of 808°/d. The gray scale indicates the wave power normalized by the average value over one rotation of the planet.

modulation rate in early 2011 has been proposed to be related to the GWS [*Fischer et al*., 2014]. Then after more than 1 year of equatorial orbits during which no modulation signal was observed for the 5 kHz narrowband emissions, the dual periodicities reappeared in 2013 as Cassini shifted to high inclination orbits and disappeared in 2014 before the orbits became equatorial. However, we cannot tell which hemisphere is rotating faster in 2013 by analyzing narrowband emission data, due to the indistinguishable hemispheric origins of these emissions as described above.

Figure 5 shows the phase plot of the 5 kHz narrowband emissions, where the intensity maxima (white) can be identified with the help of the directional statistics (magenta star symbols). We can also determine the modulation rates using the phase tracing method described above. As narrowband emissions are not separable by the hemisphere of origin, we made the phase plot based on the total power of narrowband emissions. Comparing the phase plot to the modulation spectrogram, it is clear that strong modulation signals are observed when the striation patterns are evident in the phase plot, i.e., mainly in 2013. The dual periods of narrowband emission correspond to the two possible ways of tracing the intensity maxima of narrowband emissions in the phase plot, indicated by two sets of blue lines. The steep negative slope phase tracing corresponds to a modulation rate faster than the guide rate and the almost horizontal one corresponds to a rate close to the guide rate. The two modulation rates derived from phase tracing (~808°/d and ~812°/d) are consistent with the two strong rotation signals in 2013 in the modulation spectrogram of narrowband emissions.

4. Auroral Hiss

Broadband whistler mode emissions commonly observed by the Cassini spacecraft at high latitudes in Saturn's magnetosphere at frequencies below about 100 Hz have characteristics very similar to auroral hiss observed at high latitudes in Earth's magnetosphere. Saturn auroral hiss shows a very pronounced rotational modulation, and the rotational periods matched those of SKR in the northern and southern hemispheres of Saturn [*Gurnett et al*., 2009b]. The similar north-south difference in the rotation rates of Saturn auroral hiss provides strong confirmation of a fundamental north-south asymmetry in the rotation rates of auroral phenomena at Saturn.

Saturn auroral hiss is generated by upward traveling electrons in the downward current region of the auroral current system. Unlike SKR and narrowband emissions, which are free space-propagating *R*-*X*-mode and *L*-*O*-mode emissions, the whistler mode auroral hiss can only propagate along the resonance cone and below the local plasma frequency or the local electron cyclotron frequency, whichever is lower. The raypaths form a funnel shape centered on the source field-aligned current. Therefore, the spacecraft has to cut across the funnel-shaped raypath of auroral hiss to detect the emission. This has two major consequences: auroral hiss can only be observed at high latitudes and the rotational signals associated with auroral hiss cannot cross the equator.

Since Saturn auroral hiss is emitted by the downward current, which rotates with the planet, it behaves more like a rotating beam than a clock [*Gurnett et al*., 2009b]. Therefore, we use the longitude of the spacecraft to

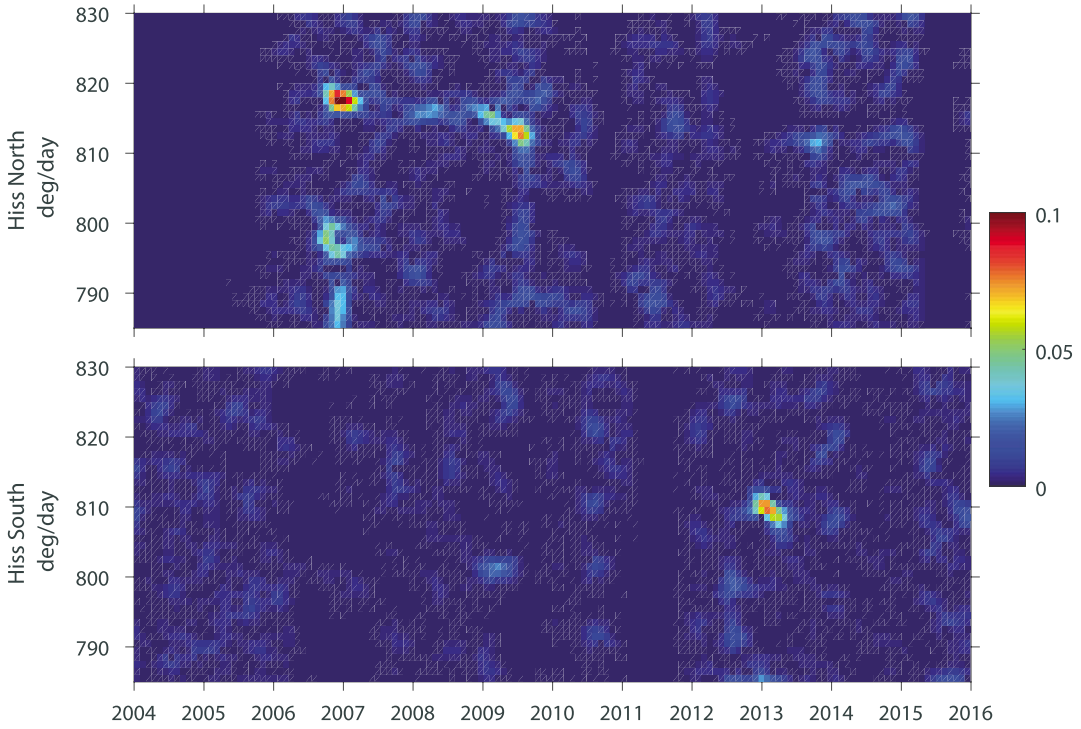

Figure 6. Least squares spectral analysis (similar to the tracking filter analysis) of the north and south auroral hiss power, separated by latitude of observation, from 2004 to 2016. The auroral hiss powers were sorted into bins of longitude of the spacecraft before the least squares fits. The color shows the square of the peak-to-peak amplitude of the fitted wave power modulation.

bin the power of Saturn auroral hiss and apply the least squares spectral analysis (similar to the tracking filter method used by *Gurnett et al.* [2011a]) to generate the modulation spectrogram. Figure 6 shows the modulation spectrograms of Saturn auroral hiss in the northern and southern hemispheres. The power of auroral hiss is integrated between 2 and 30 Hz, and the northern and southern components are separated based on the latitude of Cassini. The modulation of auroral hiss is only observed during the high inclination orbits of Cassini. The northern and southern rotation signals are well separated by restricting the latitude of observation (e.g., latitude $> 10°$ for north auroral hiss and latitude $< -10°$ for south auroral hiss). The determined auroral hiss modulation rates display similar north-south asymmetry as SKR before mid-2009, consistent with the results of *Gurnett et al.* [2009b]. Note that the rotational modulation rate for the southern auroral hiss in early 2013 is around 810°/d, which corresponds to the strong southern SKR signal at that time. There is only a very weak northern auroral hiss modulation signal after Saturn equinox in late 2013, around 812°/d. There is no clear corresponding northern SKR signal. The weak signal is usually due to the limitation in the amount of time Cassini spent in that particular hemisphere, because auroral hiss propagates within a narrow cone along the source magnetic field line and the spacecraft has to cut through the cone to observe it.

Figure 7 shows the phase plots of Saturn auroral hiss (2012–2016) in the northern and southern hemispheres based on a guide rate of 808°/d. From the intensity patterns in the phase plots, we can deduce the rotation rates of Saturn auroral hiss by measuring the slopes of the stripe patterns. A negative slope indicates a rotation rate higher than the guide rate, whereas a positive slope indicates a rotation rate lower than the guide rate. The stripe patterns only occur during the high spacecraft latitude period, from mid-2012 to early 2015. The blue lines show semiautomated computer tracing of the intensity maxima of auroral hiss, guided by directional statistics (magenta stars), and similar to what was done for SKR. The phase pattern of the north auroral hiss is not evident for most of 2013 and only starts to become clear in late 2013/early 2014 when Cassini spent more time in the northern hemisphere. This is vice versa for south auroral hiss which shows no clear pattern after late 2013. This is consistent with the intensities of the modulation signals in the modulation spectrograms (see Figure 6).

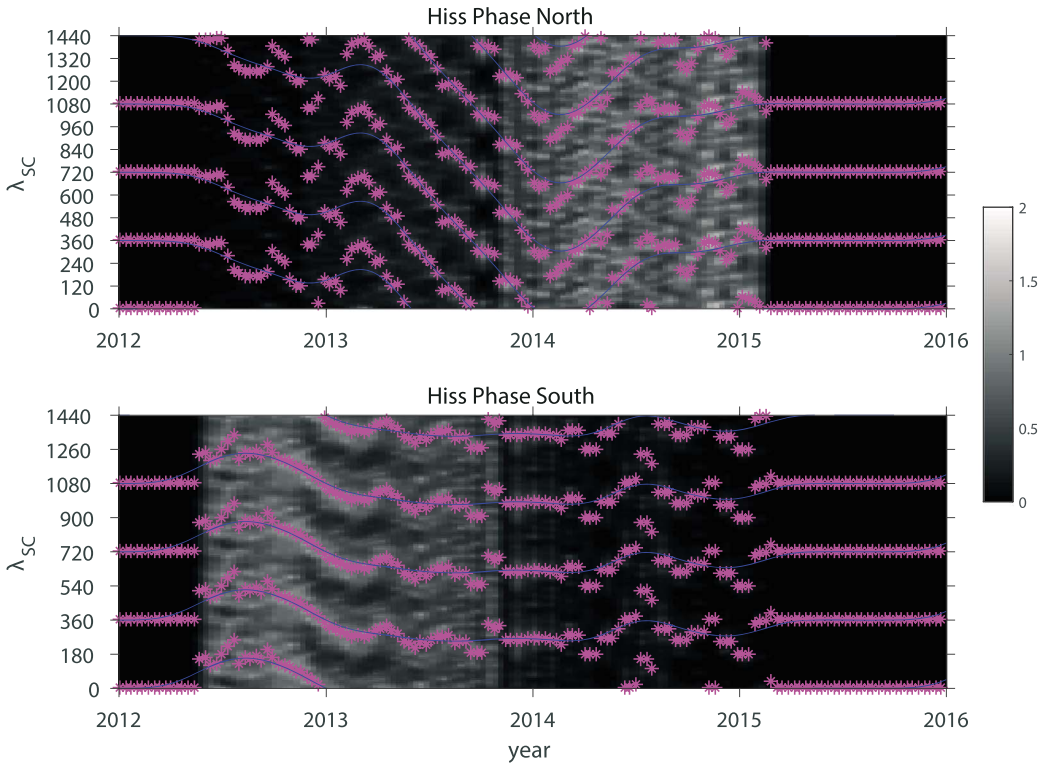

Figure 7. Phase tracing for the north and south auroral hiss. The longitude of the spacecraft is calculated based on a fixed guiding rate of 808°/d. Blue lines show the ways the intensity maxima of the north and south auroral hiss were traced with a computer algorithm. The gray scale indicates the wave power normalized by the average value over one rotation of the planet.

The rotation rates of auroral hiss derived from phase tracing are compared with those of SKR and narrowband emissions in Figure 8. There is a general agreement among all three emissions at the beginning of 2013, after which the two SKR rotation rates start to converge and the two rates stay close to each other for about 1 year. The SKR rates derived from phase tracing agree with the Lomb-Scargle analysis result. The rotation rates of auroral hiss agree with those of narrowband emissions when both are observable during the high inclination orbits in 2013/early 2014. However, the rotation rate of north auroral hiss decreases sharply in 2014, crossing the rotation rate of south auroral hiss around 808°/d. There are some weak modulation signals in Figure 6 (top) that could correspond to this sharp decrease of north auroral hiss rotation rate in 2014. The two rotation rates of the narrowband emission seem to stay parallel to each other until the end of 2013. This discrepancy in rotation rates between the three emissions is not understood.

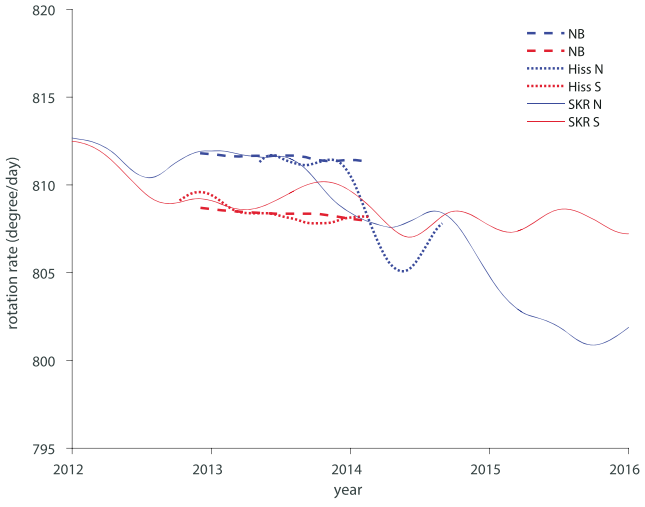

Figure 8. Comparison of the rotation rates of SKR, narrowband emissions, and auroral hiss, derived from phase tracings.

5. Discussion

The rotational modulation analysis of three types of emissions from Saturn's magnetosphere, SKR, narrowband emission, and auroral hiss, showed that these

emissions are modulated at similar periods, which are variable at the timescale of a Saturn year. The long-term variations in periodicities are mostly likely due to seasonal changes in the polar regions of each hemisphere, as the rotational modulation of the emissions also displays a hemispheric asymmetry that turns around after each equinox. The strength of the field-aligned current, which controls the intensities of the emissions, is determined by the ionospheric conductivity. The solar EUV ionization in each polar ionosphere is subject to seasonal change as the Sun elevation angle in the polar region changes over a Saturn year. The neutral atmospheric winds in the auroral zone, which are also subject to seasonal changes, could influence the slippage of the magnetosphere over the neutral atmosphere, which causes the variation of the periods observed in radio emissions and magnetic field perturbations [*Smith*, 2006]. However, the fact that the modulation periods of the radio emissions and magnetic field perturbations remained coalesced or nearly coalesced until 5 years after the recent equinox (rather than a clean reversal as observed by Ulysses after the last equinox) remains unexplained. One difference between the recent equinox and the last is the 2010 GWS, which is a source of gravity waves that could disrupt the neutral wind system globally and keep the two hemispheres symmetric [*Fischer et al*., 2014], but its effect would have to last much longer than the GWS itself.

A recent global MHD model by *Jia et al*. [2012] successfully reproduced many of the observed rotational variations in Saturn's magnetosphere by postulating double vortices in Saturn's auroral ionospheres. Although the origin of these vortices was not explained by *Jia et al*. [2012] or *Jia and Kivelson* [2012], and there is no observational evidence of such vortices so far, the idea of having the driving source in the polar region is consistent with the observed hemispherical asymmetry and seasonal variations of the SKR rotation periods [*Gurnett et al*., 2009a; *Gurnett*, 2010]. *Cowley and Provan* [2013] explored the relations between the rotation periods of the magnetic field perturbations and tropospheric/stratospheric features of the neutral atmosphere of Saturn, but they found no clear link. *Smith* [2014] suggested that the vortices should be in the upper atmosphere around 750 km altitude as observations show that the plasma and neutrals subcorotate in the polar ionosphere. Recently, a planetary wave model was built to explain the 10.7 h periodicities of Saturn [*Smith et al*., 2016].

The neutral atmosphere control of the field-aligned current is consistent with *Fischer et al*. [2014] who showed that the SKR periods in 2011 might have been influenced by the GWS, a giant lightning storm, which started late 2010 and lasted for several months. The GWS occurred in the northern hemisphere, which could disrupt the double vortices in the northern polar atmosphere thereby reducing the coupling current between the northern auroral ionosphere and the magnetosphere. As the field-aligned current and load on the northern hemisphere decreases, the field-aligned current and load on the southern hemisphere increases, which is consistent with the observed enhancement and slowing down of the southern SKR rotation signal in 2011. This reduction in the northern field-aligned current is also observed in the magnetic field perturbation data [*Provan et al*., 2013] during their E2 period, when the southern hemisphere magnetic field perturbation resumed dominance over the north. However, *Cowley and Provan* [2015] argued that switches in hemispheric dominance were observed after equinox at times not associated with any thunderstorm activity.

Andrews et al. [2010b] proposed model current systems, which account for the perturbation magnetic field in the core region of Saturn's magnetosphere. The current systems, one in each hemisphere, basically consist of field-aligned currents flowing into the auroral ionosphere, across the polar cap, and out of the ionosphere on the other side of the planet. The return currents flow in the equatorial plane across the magnetic field lines outside the quasi-dipolar region. This current system was modified by *Southwood and Cowley* [2014] to include currents on the boundaries of open field line regions to explain the origin of the periodic magnetic perturbations of Saturn as being imposed independently from the north and south polar regions. *Hunt et al*. [2014, 2015] analyzed the field-aligned current system in greater detail. The overall current layer colatitude is found to modulate with a 1° amplitude with the planetary rotation period, which could be related to the oscillation of the plasmapause-like boundary studied by *Gurnett et al*. [2011b] and the oscillatory motion of the auroral oval observed by *Nichols et al*. [2008]. The evolution of the current layer locations with planetary rotation phase indicates that the planetary period oscillation current system is driven outward from the neutral atmosphere rather than inward from the magnetosphere [*Hunt et al*., 2014].

It is known that SKR is generated on auroral field lines in the upward current region, whereas auroral hiss is generated by electrons moving up the auroral field line in the downward current region [*Gurnett et al*., 2009a,

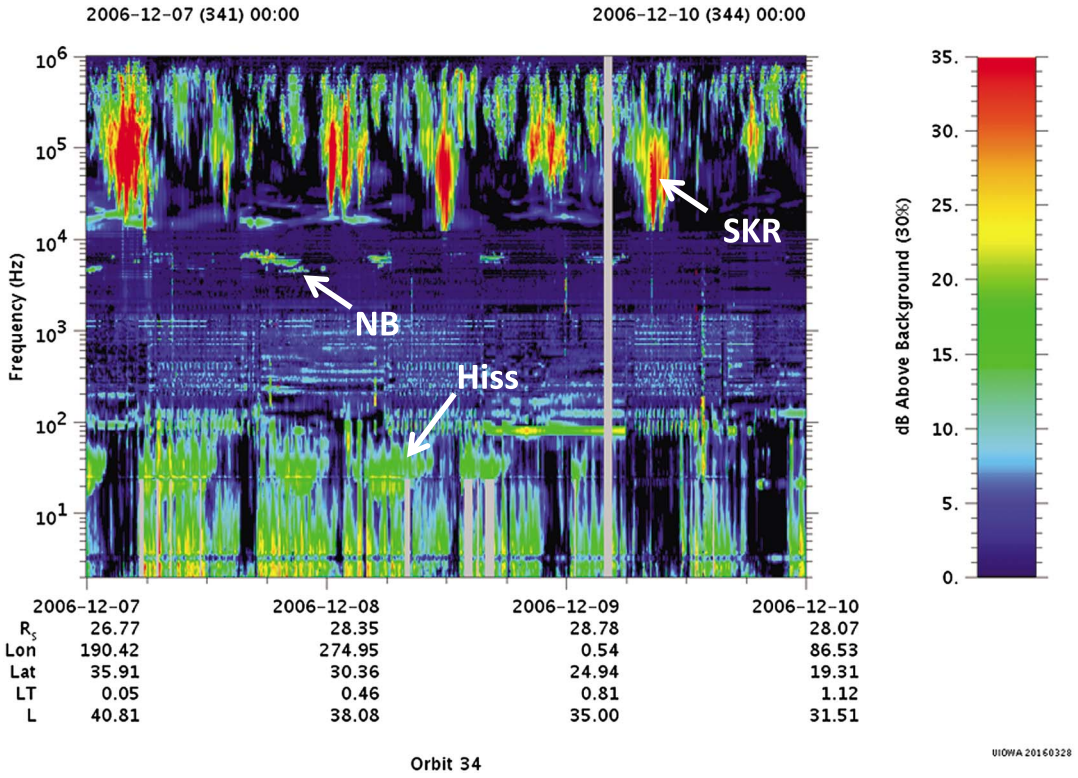

Figure 9. RPWS spectrogram showing the modulation and relative phase between SKR, narrowband emission, and auroral hiss (frequency from high to low) for a 3 day period between 7 and 10 December 2006. Cassini was around midnight local time during this period. Note that the phase difference between SKR and narrowband mission is about 90°, and auroral hiss is roughly in phase with the narrowband emissions.

2009b; *Schippers et al*., 2011]. The upward and downward current regions should be separated by roughly 180° in planetary rotation phase [*Andrews et al*., 2012; *Hunt et al*., 2014, 2015]. On the dawnside, the magnetic field lines corotating with the planet go against the solar wind, which peels back the outer L shell field lines creating azimuthal shears. This interaction between Saturn's magnetic field and solar wind intensifies the field-aligned currents. SKR is modulated like a clock (strongest source on the early morning sector), whereas auroral hiss is a rotating beam [*Gurnett et al*., 2009b]. So when comparing the phase between SKR and auroral hiss, we expect the phase difference between the two emissions to depend on the local time of Cassini. For example, on the dawnside, the phase difference between SKR and auroral hiss should be around 180°, whereas at midnight or noon local time the phase difference should be around ±90°, respectively. On the duskside, the phase difference would be either 0 or 180°, depending on whether the dominant SKR source on the morning side is viewable or not. In the latter case, SKR would look like a rotating beam to the observer. It has been shown that Saturn narrowband emission is a clock-like emission [*Wang et al*., 2010], and it lags SKR by about 90° in terms of the longitude of the Sun [*Ye et al*., 2010a]. The phase relations between these emissions are compared for two periods when Cassini was at midnight and dawn local time sectors, respectively. Figure 9 shows a RPWS spectrogram covering the time interval from 7 to 10 December 2006 (over 3 days). Cassini was around midnight local time during this period. It can be seen from this spectrogram that narrowband emission lags SKR by about 90° in phase and auroral hiss is roughly in phase with narrowband emission. The RPWS spectrogram in Figure 10 shows the phase relation between SKR and auroral hiss for the time period from 29 January to 3 February 2007 (over 5 days). During this time the local time of Cassini changed from 02 LT to 13 LT. Note that SKR and auroral hiss are almost in antiphase in the predawn local time sector.

We also found a local time dependence for the observed intensity of auroral hiss, indicating that it also acts like a strobe. Figure 11 (top) shows the auroral hiss intensity as a function of local time and L shell. The electric field wave powers are integrated over the auroral hiss frequency range (2 to 30 Hz) and averaged within each hour local time and L shell bin (for observations more than 10° above or below the equator between 2005

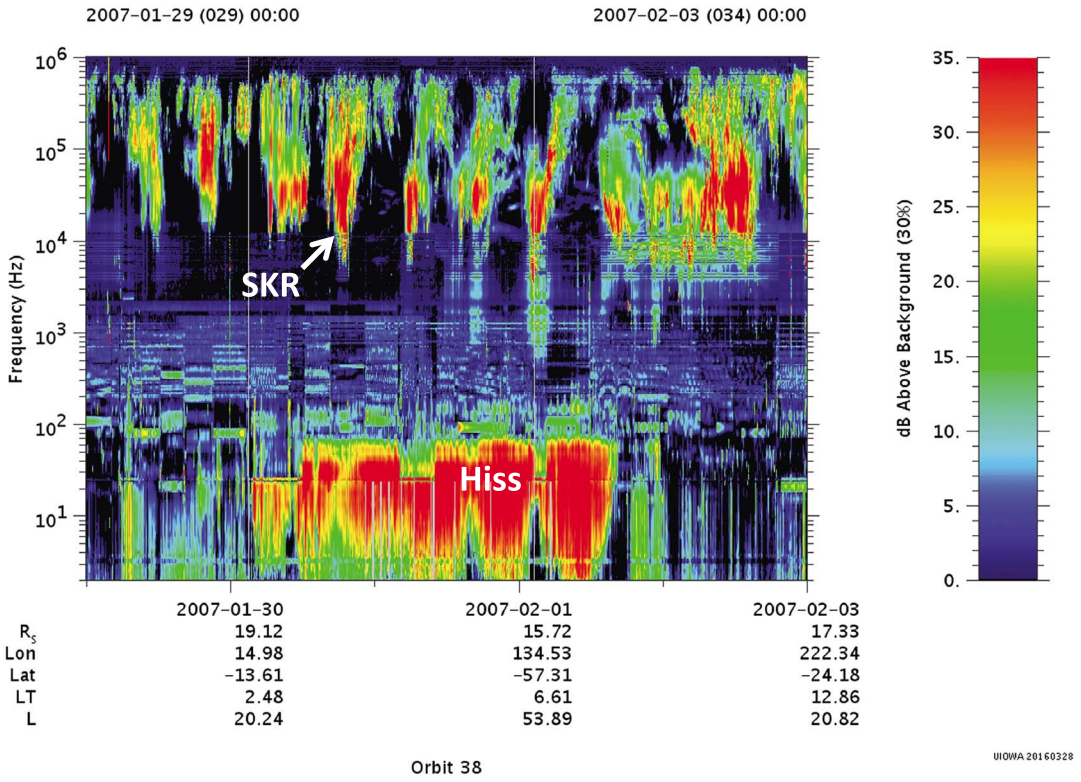

Figure 10. RPWS spectrogram showing the modulation and relative phase of SKR and auroral hiss for a 5 day period from 29 January to 3 February 2007. Cassini was around predawn local time when auroral hiss was observed. Note that SKR and auroral hiss are almost in antiphase in the predawn local time sector.

and 2015). It is shown that the observed intensities of auroral hiss are higher at dawn and dusk sectors throughout midnight. Figure 11 (bottom) shows the total time of observation within each local time and L shell bin. It shows that the local time L shell space was well covered except around 11–12 LT at large L shells (>38) and 14–22 LT at very small L shells (<4). The local time preference of the average power of auroral hiss might indicate that auroral hiss is more like a flashing light, which intensifies at certain local time sectors during each rotation. The Saturn auroral hiss may only appear to be a searchlight due to its narrow emission cone. However, one could interpret Figure 11 also as a dayside and nightside asymmetry, where due to an unknown reason, auroral hiss is roughly absent around noon at $L < 25$. We have also checked the spatial dependence of auroral hiss power within each hemisphere, which showed similar local time and L shell dependence. The intensification of auroral hiss on the dawnside and duskside is consistent with the rotating field-aligned currents intensifying on the dawnside due to the interaction of Saturn's magnetic field with the solar wind. The dawnside upward current, responsible for the generation of SKR, draws downward current on the other side of the planet through the polar ionosphere, which leads to intensification of auroral hiss on the duskside.

6. Summary

We analyzed the rotational modulation of SKR, auroral hiss, and narrowband emission from 2004 to the end of 2015 with a focus on the years from 2012 to the end of 2015. The Lomb-Scargle analysis of polarization-separated SKR power time series showed that the northern SKR rotation slowed to ~802°/d, whereas the southern SKR rotation remained at ~808°/d in 2015. The phase analysis of the northern and southern SKR showed that the rotation rates of these two SKR components are different since mid-2012 with SKR north being faster until late 2013. This was followed by a 1 year interval of similar north and south rotation rates and phases, before north SKR finally became slower than south SKR in late 2014. The Lomb-Scargle analysis of the 5 kHz narrowband emissions showed signs of dual rotation rates (hemispherical origins not distinguishable) in 2013 again, which agree with SKR modulation rates in early 2013. The hemispherical origins

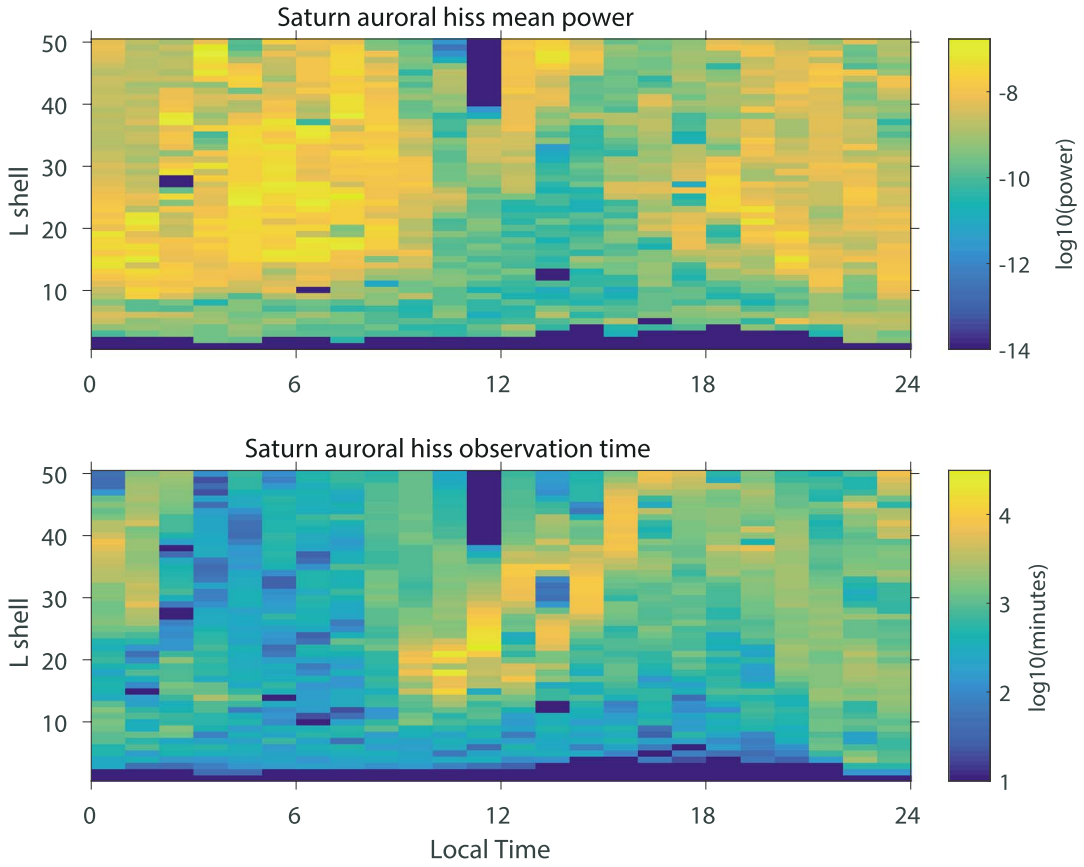

Figure 11. Local time and L shell dependence of auroral hiss intensity. (top) Logarithm of the average power of auroral hiss as a function of local time and L shell. The wave power is integrated between 2 and 30 Hz and sorted into local time and L shell bins. (bottom) Distribution of the amount of time Cassini spent within each local time and L shell bin (for the absolute value of Cassini latitude greater than 10°).

of auroral hiss are distinguishable by the latitude of observation. Least squares spectral analysis applied to auroral hiss power time series showed distinct periods in the northern and southern hemispheres, which are consistent with SKR before mid-2013 but are slightly different afterward. However, auroral hiss and narrowband emission showed agreement in modulation rates in 2013 despite the ambiguity in the hemispherical origin of narrowband emissions. We also showed a strong dependence of auroral hiss intensity on local time, characteristics of clock-like modulation or an inherent dayside and nightside asymmetry. Phase comparisons between SKR and auroral hiss showed that the phase difference between the two emissions depends on the local time of Cassini. The source field-aligned currents of SKR and auroral hiss rotate with the planet but intensify when they pass through the dawn/morning sector. The local time dependence of the phase difference between SKR and auroral hiss is probably due to the narrow beaming of auroral hiss; i.e., the emission is only visible when Cassini is passing through the emission cone. However, statistically, auroral hiss is much more intense (by about 2 orders of magnitude) when observed at dawn and dusk compared to observations around noon.

Acknowledgments
This research was supported by NASA through contract 1415150 with the Jet Propulsion Laboratory. The data used in this study are available through the Planetary Data System or from the authors. The paper also benefited from the discussions in the international team workshop "Rotational phenomena in Saturn's magnetosphere" funded by the International Space Science Institute (ISSI) in Bern, Switzerland.

References

Andrews, D. J., E. J. Bunce, S. W. H. Cowley, M. K. Dougherty, G. Provan, and D. J. Southwood (2008), Planetary period oscillations in Saturn's magnetosphere: Phase relation of equatorial magnetic field oscillations and Saturn kilometric radiation modulation, *J. Geophys. Res.*, *113*, A09205, doi:10.1029/2007JA012937.

Andrews, D. J., S. W. H. Cowley, M. K. Dougherty, and G. Provan (2010a), Magnetic field oscillations near the planetary period in Saturn's equatorial magnetosphere: Variation of amplitude and phase with radial distance and local time, *J. Geophys. Res.*, *115*, A04212, doi:10.1029/2009JA014729.

Andrews, D. J., A. J. Coates, S. W. H. Cowley, M. K. Dougherty, L. Lamy, G. Provan, and P. Zarka (2010b), Magnetospheric period oscillations at Saturn: Comparison of equatorial and high-latitude magnetic field periods with north and south Saturn kilometric radiation periods, *J. Geophys. Res.*, *115*, A12252, doi:10.1029/2010JA015666.

Andrews, D. J., B. Cecconi, S. W. H. Cowley, M. K. Dougherty, L. Lamy, G. Provan, and P. Zarka (2011), Planetary period oscillations in Saturn's magnetosphere: Evidence in magnetic field phase data for rotational modulation of Saturn kilometric radiation emissions, *J. Geophys. Res.*, *116*, A09206, doi:10.1029/2011JA016636.

Andrews, D. J., S. W. H. Cowley, M. K. Dougherty, L. Lamy, G. Provan, and D. J. Southwood (2012), Planetary period oscillations in Saturn's magnetosphere: Evolution of magnetic oscillation properties from southern summer to post-equinox, *J. Geophys. Res.*, *117*, A04224, doi:10.1029/2011JA017444.

Carbary, J. F., D. G. Mitchell, S. M. Krimigis, and N. Krupp (2009), Dual periodicities in energetic electrons at Saturn, *Geophys. Res. Lett.*, *36*, L20103, doi:10.1029/2009GL040517.

Carbary, J. F., D. G. Mitchell, S. M. Krimigis, and N. Krupp (2011), Post-equinox periodicities in Saturn's energetic electrons, *Geophys. Res. Lett.*, *38*, L24104, doi:10.1029/2011GL050259.

Clarke, K. E., et al. (2006), Cassini observations of planetary-period oscillations of Saturn's magnetopause, *Geophys. Res. Lett.*, *33*, L23104, doi:10.1029/2006GL027821.

Clarke, K. E., D. J. Andrews, C. S. Arridge, A. J. Coates, and S. W. H. Cowley (2010a), Magnetopause oscillations near the planetary period at Saturn: Occurrence, phase, and amplitude, *J. Geophys. Res.*, *115*, A08209, doi:10.1029/2009JA014745.

Clarke, K. E., D. J. Andrews, A. J. Coates, S. W. H. Cowley, and A. Masters (2010b), Magnetospheric period oscillations of Saturn's bow shock, *J. Geophys. Res.*, *115*, A05202, doi:10.1029/2009JA015164.

Cowley, S. W. H., and G. Provan (2013), Saturn's magnetospheric planetary period oscillations, neutral atmosphere circulation, and thunderstorm activity: Implications, or otherwise, for physical links, *J. Geophys. Res, Space Physics*, *118*, 7246–7261, doi:10.1002/2013JA019200.

Cowley, S. W., and G. Provan (2015), Planetary period oscillations in Saturn's magnetosphere: Comments on the relation between post-equinox periods determined from magnetic field and SKR emission data, doi:10.5194/angeo-33-901-2015.

Cowley, S. W. H., and G. Provan (2016), Planetary period oscillations in Saturn's magnetosphere: Further comments on the relation between post-equinox properties deduced from magnetic field and Saturn kilometric radiation measurements, *Icarus*, *272*, 258–276, doi:10.1016/j.icarus.2016.02.051.

Desch, M. D., and M. L. Kaiser (1981), Voyager measurement of the rotation period of Saturn's magnetic field, *Geophys. Res. Lett.*, *8*, 253–256, doi:10.1029/GL008i003p00253.

Fischer, G., S. Y. Ye, J. B. Groene, A. P. Ingersoll, K. M. Sayanagi, J. D. Menietti, W. S. Kurth, and D. A. Gurnett (2014), A possible influence of the Great White Spot on Saturn kilometric radiation periodicity, *Ann. Geophys.*, *32*, 1463–1476, doi:10.5194/angeo-32-1463-2014.

Fischer, G., D. A. Gurnett, W. S. Kurth, S. Y. Ye, and J. B. Groene (2015), Saturn kilometric radiation periodicity after equinox, *Icarus*, *254*, 72–91, doi:10.1016/j.icarus.2015.03.014.

Galopeau, P. H., and A. Lecacheux (2000), Variations of Saturn's radio rotation period measured at kilometer wavelengths, *J. Geophys. Res.*, *105*, 13,089–13,101, doi:10.1029/1999JA005089.

Gurnett, D. A.et al. (2010), A plasmapause-like density boundary at high latitudes in Saturn's magnetosphere, *Geophys. Res. Lett.*, *37*, L16806, doi:10.1029/2010GL044466.

Gurnett, D. A., et al. (2005), Radio and plasma wave observations at Saturn from Cassini's approach and first orbit, *Science*, *307*(5713), 1255–1259, doi:10.1126/science.1105356.

Gurnett, D. A., A. M. Persoon, W. S. Kurth, J. B. Groene, T. F. Averkamp, M. K. Dougherty, and D. J. Southwood (2007), The variable rotation period of the inner region of Saturn's plasma disk, *Science*, *316*(5823), 442–445, doi:10.1126/science.1138562.

Gurnett, D. A., A. Lecacheux, W. S. Kurth, A. M. Persoon, J. B. Groene, L. Lamy, P. Zarka, and J. F. Carbary (2009a), Discovery of a north-south asymmetry in Saturn's radio rotation period, *Geophys. Res. Lett.*, *36*, L16102, doi:10.1029/2009GL039621.

Gurnett, D. A., A. M. Persoon, J. B. Groene, A. J. Kopf, G. B. Hospodarsky, and W. S. Kurth (2009b), A north-south difference in the rotation rate of auroral hiss at Saturn: Comparison to Saturn's kilometric radio emission, *Geophys. Res. Lett.*, *36*, L21108, doi:10.1029/2009GL040774.

Gurnett, D. A., J. B. Groene, A. M. Persoon, J. D. Menietti, S. Y. Ye, W. S. Kurth, R. J. MacDowall, and A. Lecacheux (2010a), The reversal of the rotational modulation rates of the north and south components of Saturn kilometric radiation near equinox, *Geophys. Res. Lett.*, *37*, L24101, doi:10.1029/2010GL045796.

Gurnett, D. A., J. B. Groene, T. F. Averkamp, W. S. Kurth, S. Y. Ye, and G. Fischer (2011a), An SLS4 longitude system based on a tracking filter analysis of the rotational modulation of Saturn kilometric radiation, in, in *Planetary Radio Emissions VII*, pp. 51–64, Austrian Academy of Sci. Press, Vienna.

Gurnett, D. A., A. M. Persoon, J. B. Groene, W. S. Kurth, M. Morooka, J.-E. Wahlund, and J. D. Nichols (2011b), The rotation of the plasmapause-like boundary at high latitudes in Saturn's magnetosphere and its relation to the eccentric rotation of the northern and southern auroral ovals, *Geophys. Res. Lett.*, *38*, L21203, doi:10.1029/2011GL049547.

Hunt, G. J., S. W. H. Cowley, G. Provan, E. J. Bunce, I. I. Alexeev, E. S. Belenkaya, V. V. Kalegaev, M. K. Dougherty, and A. J. Coates (2014), Field-aligned currents in Saturn's southern nightside magnetosphere: Subcorotation and planetary period oscillation components, *J. Geophys. Res. Space Physics*, *119*, 9847–9899, doi:10.1002/2014JA020506.

Hunt, G. J., S. W. H. Cowley, G. Provan, E. J. Bunce, I. I. Alexeev, E. S. Belenkaya, V. V. Kalegaev, M. K. Dougherty, and A. J. Coates (2015), Field-aligned currents in Saturn's northern nightside magnetosphere: Evidence for interhemispheric current flow associated with planetary period oscillations, *J. Geophys. Res. Space Physics*, *120*, 7552–7584, doi:10.1002/2015JA021454.

Jia, X., and M. G. Kivelson (2012), Driving Saturn's magnetospheric periodicities from the upper atmosphere/ionosphere: Magnetotail response to dual sources, *J. Geophys. Res.*, *117*, A11219, doi:10.1029/2012JA018183.

Jia, X., M. G. Kivelson, and T. I. Gombosi (2012), Driving Saturn's magnetospheric periodicities from the upper atmosphere/ionosphere, *J. Geophys. Res.*, *117*, A04215, doi:10.1029/2011JA017367.

Kimura, T., et al. (2013), Long-term modulations of Saturn's auroral radio emissions by the solar wind and seasonal variations controlled by the solar ultraviolet flux, *J. Geophys. Res. Space Physics*, *118*, 7019–7035, doi:10.1002/2013JA018833.

Kivelson, M. G., and X. Jia (2014), Control of periodic variations in Saturn's magnetosphere by compressional waves, *J. Geophys. Res. Space Physics*, *119*, 8030–8045, doi:10.1002/2014JA020258.

Kurth, W. S., A. Lecacheux, T. F. Averkamp, J. B. Groene, and D. A. Gurnett (2007), A Saturnian longitude system based on a variable kilometric radiation period, *Geophys. Res. Lett.*, *34*, L02201, doi:10.1029/2006GL028336.

Kurth, W. S., T. F. Averkamp, D. A. Gurnett, J. B. Groene, and A. Lecacheux (2008), An update to a Saturnian longitude system based on kilometric radio emissions, *J. Geophys. Res.*, *113*, A05222, doi:10.1029/2007JA012861.

Kurth, W. S., et al. (2011), A close encounter with a Saturn kilometric radiation source region, in, in *Planetary Radio Emissions VII*, pp. 75–85, Austrian Academy of Sci. Press, Vienna.

Lamy, L. (2011), Variability of southern and northern Saturn kilometric radiation periodicities, in, in *Planetary Radio Emissions VII*, pp. 39–50, Austrian Academy of Sci. Press, Vienna.

Lamy, L., et al. (2010), Properties of Saturn kilometric radiation measured within its source region, *Geophys. Res. Lett.*, *37*, L12104, doi:10.1029/2010GL043415.

Lamy, L., R. Prangé, W. Pryor, J. Gustin, S. V. Badman, H. Melin, T. Stallard, D. G. Mitchell, and P. C. Brandt (2013), Multispectral simultaneous diagnosis of Saturn's aurorae throughout a planetary rotation, *J. Geophys. Res. Space Physics*, *118*, 4817–4843, doi:10.1002/jgra.50404.

Lecacheux, A., P. Galopeau, and M. Aubier (1997), Re-visiting Saturnian kilometric radiation with Ulysses/URAP, in, in *Planetary Radio Emissions IV*, pp. 313–325, Austrian Academy of Sci. Press, Vienna.

Lomb, N. R. (1976), Least-squares frequency analysis of unequally spaced data, *Astrophys. Space Sci.*, *39*(2), 447–462, doi:10.1007/BF00648343.

Menietti, J. D., S. Y. Ye, P. H. Yoon, O. Santolik, A. M. Rymer, D. A. Gurnett, and A. J. Coates (2009), Analysis of narrowband emission observed in the Saturn magnetosphere, *J. Geophys. Res.*, *114*, A06206, doi:10.1029/2008JA013982.

Menietti, J. D., P. H. Yoon, S. Y. Ye, B. Cecconi, and A. M. Rymer (2010), Source mechanism of Saturn narrowband emission, *Ann. Geophys.*, *28*, 1013–1021, doi:10.5194/angeo-28-1013-2010.

Menietti, J. D., R. L. Mutel, P. Schippers, S. Y. Ye, O. Santolik, W. S. Kurth, D. A. Gurnett, L. Lamy, and B. Cecconi (2011), Saturn kilometric radiation near a source center on day 73, 2008, in, in *Planetary Radio Emissions VII*, pp. 87–95, Austrian Academy of Sci. Press, Vienna.

Mitchell, D. G., et al. (2009), Recurrent energization of plasma in the midnight-to-dawn quadrant of Saturn's magnetosphere, and its relationship to auroral UV and radio emissions, *Planet. Space Sci.*, *57*(14), 1732–1742, doi:10.1016/j.pss.2009.04.002.

Nichols, J. D., J. T. Clarke, S. W. H. Cowley, J. Duval, A. J. Farmer, J. C. Gérard, D. Grodent, and S. Wannawichian (2008), Oscillation of Saturn's southern auroral oval, *J. Geophys. Res.*, *113*, A11205, doi:10.1029/2008JA013444.

Nichols, J. D., B. Cecconi, J. T. Clarke, S. W. H. Cowley, J. C. Gérard, A. Grocott, D. Grodent, L. Lamy, and P. Zarka (2010a), Variation of Saturn's UV aurora with SKR phase, *Geophys. Res. Lett.*, *37*, L15102, doi:10.1029/2010GL044057.

Nichols, J. D., S. W. H. Cowley, and L. Lamy (2010b), Dawn-dusk oscillation of Saturn's conjugate auroral ovals, *Geophys. Res. Lett.*, *37*, L24102, doi:10.1029/2010GL045818.

Press, W. H. (2007), *Numerical Recipes 3rd Edition: The Art of Scientific Computing*, Cambridge Univ. Press, New York.

Provan, G., D. J. Andrews, B. Cecconi, S. W. H. Cowley, M. K. Dougherty, L. Lamy, and P. Zarka (2011), Magnetospheric period magnetic field oscillations at Saturn: Equatorial phase "jitter" produced by superposition of southern and northern period oscillations, *J. Geophys. Res.*, *116*, A04225, doi:10.1029/2010JA016213.

Provan, G., D. J. Andrews, C. S. Arridge, A. J. Coates, S. W. H. Cowley, G. Cox, M. K. Dougherty, and C. M. Jackman (2012), Dual periodicities in planetary-period magnetic field oscillations in Saturn's tail, *J. Geophys. Res.*, *117*, A01209, doi:10.1029/2011JA017104.

Provan, G., S. W. H. Cowley, J. Sandhu, D. J. Andrews, and M. K. Dougherty (2013), Planetary period magnetic field oscillations in Saturn's magnetosphere: Postequinox abrupt nonmonotonic transitions to northern system dominance, *J. Geophys. Res. Space Physics*, *118*, 3243–3264, doi:10.1002/jgra.50186.

Provan, G., C. Tao, S. W. H. Cowley, M. K. Dougherty, and A. J. Coates (2015), Planetary period oscillations in Saturn's magnetosphere: Examining the relationship between abrupt changes in behavior and solar wind-induced magnetospheric compressions and expansions, *J. Geophys. Res. Space Physics*, *120*, 9524–9544, doi:10.1002/2015JA021642.

Rymer, A. M., D. G. Mitchell, T. W. Hill, E. A. Kronberg, N. Krupp, and C. M. Jackman (2013), Saturn's magnetospheric refresh rate, *Geophys. Res. Lett.*, *40*, 2479–2483, doi:10.1002/grl.50530.

Scargle, J. D. (1982), Studies in astronomical time series analysis. II—Statistical aspects of spectral analysis of unevenly spaced data, *Astrophys. J.*, *263*, 835–853, doi:10.1086/160554.

Schippers, P., et al. (2011), Auroral electron distributions within and close to the Saturn kilometric radiation source region, *J. Geophys. Res.*, *116*, A05203, doi:10.1029/2011JA016461.

Smith, C. G. A. (2006), Periodic modulation of gas giant magnetospheres by the neutral upper atmosphere, *Ann. Geophys.*, *24*(10), 2709–2717, doi:10.5194/angeo-24-2709-2006.

Smith, C. G. A. (2014), On the nature and location of the proposed twin vortex systems in Saturn's polar upper atmosphere, *J. Geophys. Res, Space Physics*, *119*, 5964–5977, doi:10.1002/2014JA019934.

Smith, C. G. A., L. C. Ray, and N. A. Achilleos (2016), A planetary wave model for Saturn's 10.7-h periodicities, *Icarus*, *268*, 76–88, doi:10.1016/j.icarus.2015.12.041.

Southwood, D. J., and S. W. H. Cowley (2014), The origin of Saturn's magnetic periodicities: Northern and southern current systems, *J. Geophys. Res. Space Physics*, *119*, 1563–1571, doi:10.1002/2013JA019632.

Wang, Z., D. A. Gurnett, G. Fischer, S. Y. Ye, W. S. Kurth, D. G. Mitchell, J. S. Leisner, and C. T. Russell (2010), Cassini observations of narrowband radio emissions in Saturn's magnetosphere, *J. Geophys. Res.*, *115*, A06213, doi:10.1029/2009JA014847.

Warwick, J. W., et al. (1981), Planetary radio astronomy observations from Voyager 1 near Saturn, *Science*, *212*(4491), 239–243, doi:10.1126/science.212.4491.239.

Wu, C. S., and L. C. Lee (1979), A theory of the terrestrial kilometric radiation, *Astrophys. J.*, *230*, 621–626, doi:10.1086/157120.

Ye, S. Y., D. A. Gurnett, G. Fischer, B. Cecconi, J. D. Menietti, W. S. Kurth, Z. Wang, G. B. Hospodarsky, P. Zarka, and A. Lecacheux (2009), Source locations of narrowband radio emissions detected at Saturn, *J. Geophys. Res.*, *114*, A06219, doi:10.1029/2008JA013855.

Ye, S. Y., D. A. Gurnett, J. B. Groene, Z. Wang, and W. S. Kurth (2010a), Dual periodicities in the rotational modulation of Saturn narrowband emissions, *J. Geophys. Res.*, *115*, A12258, doi:10.1029/2010JA015780.

Ye, S. Y., J. D. Menietti, G. Fischer, Z. Wang, B. Cecconi, D. A. Gurnett, and W. S. Kurth (2010b), Z mode waves as the source of Saturn narrowband radio emissions, *J. Geophys. Res.*, *115*, A08228, doi:10.1029/2009JA01516.

Zarka, P., L. Lamy, B. Cecconi, R. Prangé, and H. O. Rucker (2007), Modulation of Saturn's radio clock by solar wind speed, *Nature*, *450*(7167), 265–267, doi:10.1038/nature06237.